

# Epitaxial Single-Layer MoS<sub>2</sub> on GaN with Enhanced Valley Helicity

Yi Wan, Jun Xiao, Jingzhen Li, Xin Fang, Kun Zhang, Lei Fu, Pan Li, Zhigang Song, Hui Zhang, Yilun Wang, Mervin Zhao, Jing Lu, Ning Tang, Guangzhao Ran, Xiang Zhang, Yu Ye,\* and Lun Dai\*

Engineering the substrate of 2D transition metal dichalcogenides can couple the quasiparticle interaction between the 2D material and substrate, providing an additional route to realize conceptual quantum phenomena and novel device functionalities, such as realization of a 12-time increased valley spitting in single-layer WSe<sub>2</sub> through the interfacial magnetic exchange field from a ferromagnetic EuS substrate, and band-to-band tunnel field-effect transistors with a subthreshold swing below 60 mV dec<sup>-1</sup> at room temperature based on bilayer *n*-MoS<sub>2</sub> and heavily doped *p*-germanium, etc. Here, it is demonstrated that epitaxially grown single-layer MoS<sub>2</sub> on a lattice-matched GaN substrate, possessing a type-I band alignment, exhibits strong substrate-induced interactions. The phonons in GaN quickly dissipate the energy of photogenerated carriers through electron–phonon interaction, resulting in a short exciton lifetime in the MoS<sub>2</sub>/GaN heterostructure. This interaction enables an enhanced valley helicity at room temperature ( $0.33 \pm 0.05$ ) observed in both steady-state and time-resolved circularly polarized photoluminescence measurements. The findings highlight the importance of substrate engineering for modulating the intrinsic valley carriers in ultrathin 2D materials and potentially open new paths for valleytronics and valley-optoelectronic device applications.

the physical properties of layered materials through the 2D material–substrate interaction gives a rise to a variety of fascinating physical behaviors or enhances device performances that are not possible to realize with single 2D materials.<sup>[2,3]</sup> For example, growth of wafer-scale single crystalline graphene on a lattice-matched hydrogen-terminated germanium substrate,<sup>[4]</sup> anomalously high critical temperature FeSe superconductivity through electron–phonon coupling with the SrTiO<sub>3</sub> substrate,<sup>[5]</sup> room-temperature topological magnetism of Bi<sub>2</sub>Se<sub>3</sub> through ferromagnetic exchange interaction coupled with a ferromagnetic insulator (EuS),<sup>[6]</sup> and many other exotic physics not possible in each material alone.

However, controlling the valley polarization of 2D transition metal dichalcogenides (TMDCs) via the 2D material–substrate interactions is yet to be explored. Achieving a high valley polarization is a necessity for the realization of valleytronics, which relies on the “valley-bit” for information processing, analogous

to charge and spin. So far, a variety of valleytronic devices, such as a valley Hall transistor, etc., have been realized by optically exciting the valley.<sup>[7,8]</sup> However, the optically generated valley polarization, especially at room temperature, is much smaller than the expected value from first-principles calculations.<sup>[9]</sup> While many attempts have been made to improve the valley helicity, such as modulating the sample

to charge and spin. So far, a variety of valleytronic devices, such as a valley Hall transistor, etc., have been realized by optically exciting the valley.<sup>[7,8]</sup> However, the optically generated valley polarization, especially at room temperature, is much smaller than the expected value from first-principles calculations.<sup>[9]</sup> While many attempts have been made to improve the valley helicity, such as modulating the sample

Y. Wan, J. Z. Li, X. Fang, K. Zhang, L. Fu, P. Li, Dr. Z. G. Song, Dr. H. Zhang, Y. L. Wang, Prof. J. Lu, Prof. N. Tang, Prof. G. Z. Ran, Prof. Y. Ye, Prof. L. Dai  
State Key Lab for Mesoscopic Physics and School of Physics  
Peking University  
Beijing 100871, P. R. China  
E-mail: ye\_yu@pku.edu.cn; lundai@pku.edu.cn

Prof. J. Lu, Prof. N. Tang, Prof. Y. Ye, Prof. L. Dai  
Collaborative Innovation Center of Quantum Matter  
Beijing 100871, P. R. China

J. Xiao, Dr. M. Zhao, Prof. X. Zhang  
NSF Nanoscale Science and Engineering Center  
University of California  
Berkeley, CA 94720, USA

Prof. X. Zhang  
Materials Sciences Division  
Lawrence Berkeley National Laboratory  
Berkeley, CA 94720, USA

 The ORCID identification number(s) for the author(s) of this article can be found under <https://doi.org/10.1002/adma.201703888>.

DOI: 10.1002/adma.201703888

quality,<sup>[10,11]</sup> measuring at low temperature,<sup>[9,12,13]</sup> and pumping with a near-resonant excitation,<sup>[14]</sup> the effect of substrate engineering has not been explored thoroughly. The 2D material–substrate interactions can strongly influence the valley polarization through strain, electron–electron and electron–phonon interactions, etc.

Here, we report the epitaxially oriented growth of single-layer MoS<sub>2</sub> on a lattice-matched GaN substrate via the chemical vapor deposition (CVD) method. The domain size and sample coverage can be precisely controlled by growth temperature and substrate-to-source distance. The emergence of the Raman silent mode<sup>[15–17]</sup> of pristine GaN obtained from the MoS<sub>2</sub>/GaN heterostructure indicates the strong electron–phonon coupling between single-layer MoS<sub>2</sub> and the adjacent GaN substrate, i.e. the vibration modes of GaN lattice modulate the behavior of the electrons and holes in MoS<sub>2</sub>. The single-layer MoS<sub>2</sub> on GaN exhibits an enhanced valley helicity,  $\approx 0.33 \pm 0.05$  at room temperature. The time-resolved circularly polarized photoluminescence (PL) spectra show a relatively short exciton lifetime, which is overwhelming enough to cause the enhanced valley helicity observed in the MoS<sub>2</sub>/GaN heterostructure. The scanning Kelvin probe microscopy (SKPM) and ultraviolet photoelectron spectroscopy (UPS) measurements reveal that a type-I band alignment is formed between the single-layer MoS<sub>2</sub> and GaN, indicating the energy of the excitons generated in single-layer MoS<sub>2</sub> is mainly dissipated by the lattice vibration in the adjacent GaN substrate, resulting in a decrease in the exciton lifetime, and thus an enhanced valley helicity. Our study demonstrates the presence of the efficient interlayer electron–phonon interactions in the 2D material–substrate system and the engineering of the valley polarization through this interaction, which will enable new ways to dynamically manipulate the

valley information for novel quantum phenomena in vdW heterostructures or 2D material–substrate systems.

In contrast to the typically used amorphous SiO<sub>2</sub> substrate, we used the epitaxy-ready grade *c*-plane (0001) wurtzite GaN ( $\approx 2 \mu\text{m}$ ) as the substrate during the CVD growth of single-layer MoS<sub>2</sub>. Epitaxial alignment between MoS<sub>2</sub> and GaN is feasible, because MoS<sub>2</sub> and GaN possess an in-plane crystal lattice mismatch of less than 1% ( $a_{\text{MoS}_2} = 0.316 \text{ nm}$ <sup>[18]</sup> and  $a_{\text{GaN}} = 0.319 \text{ nm}$ <sup>[19]</sup>). Recently, it has been found<sup>[20]</sup> that the GaN substrate can lattice match with single-layer MoS<sub>2</sub> and cause the multiple single-layer domains to coalesce into uniform layer with reduced grain boundaries, as shown in **Figure 1a**. In the MoS<sub>2</sub>/GaN heterostructure, MoS<sub>2</sub> triangle domains are aligned with the rotational symmetry of the *P6<sub>3</sub>mc* space group of GaN.<sup>[20]</sup> The MoS<sub>2</sub> is aligned at either 0° or 60° equivalent orientations, where the Mo atoms stack over the Ga atoms in an eclipsed fashion, in agreement with preferential stacking resulted from density functional theory (DFT) calculations in conjunction with the projector-augmented-wave potential (Figure 1b).<sup>[21]</sup> In this case, the configuration is the thermodynamic minima, and the occupation of MoS<sub>2</sub> is commensurate with GaN substrate (see Figure S1 in the Supporting Information). During the growth, vdW interaction between the GaN surface and the grown MoS<sub>2</sub> governs the formation of the initial nuclei, which constitutes the precursors of the layers. Only energetically stable nuclei are able to grow by laterally spreading through the lateral facets. This leads to an overall preferential orientation of the grown MoS<sub>2</sub> layers. The small discrepancy on the thermal expansion coefficients between MoS<sub>2</sub> ( $\alpha_{\text{MoS}_2} = 4.92 \times 10^{-6} \text{ K}^{-1}$ )<sup>[18]</sup> and GaN ( $\alpha_{\text{GaN}} = 3.95 \times 10^{-6} \text{ K}^{-1}$ )<sup>[19]</sup> allows for the stability of the epitaxial alignment and helps to release the residual strain when the sample is cooled from the

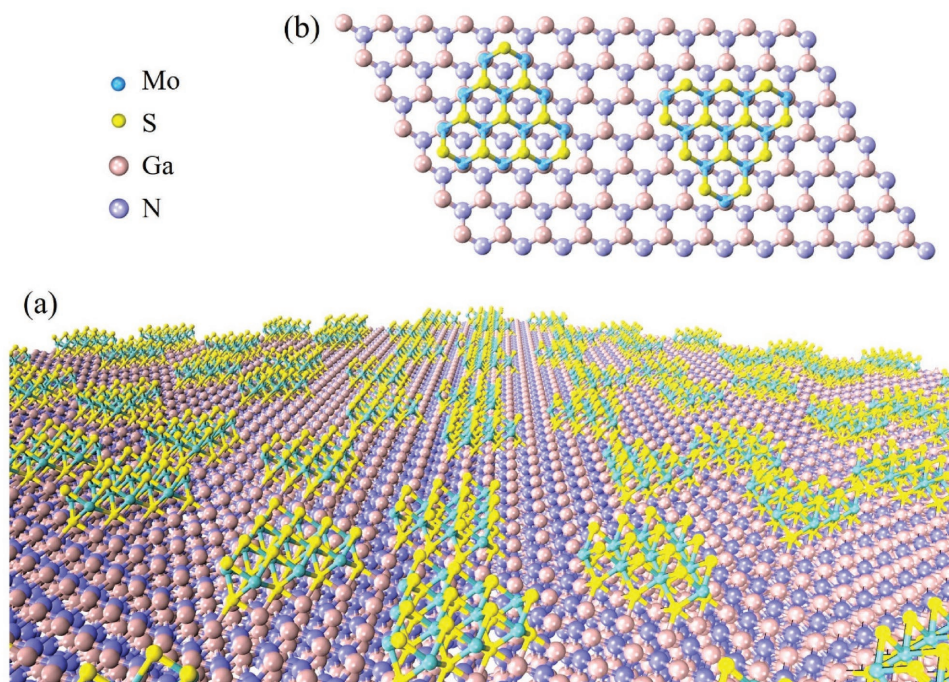


**Figure 1.** a) Schematic illustration of the heterostructure with single-layer MoS<sub>2</sub> triangles on GaN. b) Top view of the MoS<sub>2</sub>/GaN heterostructure. Based on the DFT calculations, the stacking configuration shown in (b) is the thermodynamic minima.

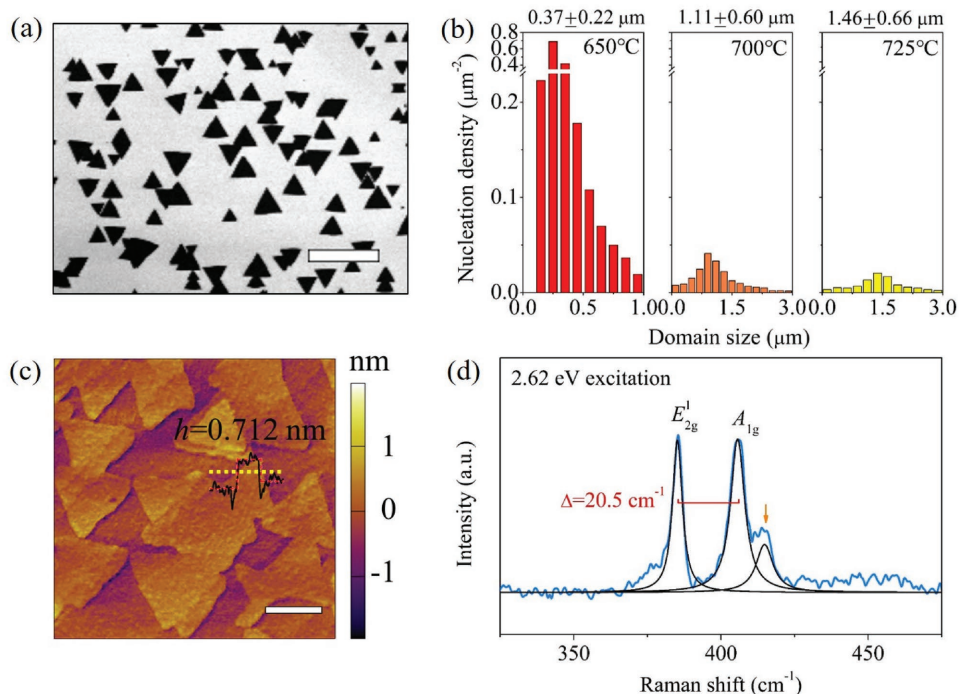


**Figure 2.** a) SEM image of epitaxial MoS<sub>2</sub> triangles grown on *n*-GaN at 700 °C. Scale bar: 5 μm. b) Statistical (including at least 300 flakes) relation of surface nucleation density with domain size for the samples grown at 650, 700, and 725 °C. c) AFM image of MoS<sub>2</sub> samples grown on GaN. Scale bar: 100 nm. d) Raman spectrum of single-layer MoS<sub>2</sub> grown on GaN. The black curves are Lorentzian fitting results.

high growth temperature to room temperature. The details of the sample synthesis are described in the Experimental Section. The initial growth morphology of MoS<sub>2</sub> on *n*-GaN substrate is analyzed by scanning electron microscopy (SEM) (Figure 2a). The darker-contrast triangle-like single crystals on the surface signify MoS<sub>2</sub>, and the surrounding regions correspond to the GaN substrate. The majority of MoS<sub>2</sub> triangles keep a long-range ordered relation, showing the relative orientation of flake edges can be expressed as multiples of 60°. The atomically smooth surface of *n*-GaN (roughness of 0.74 nm) is crucial for the epitaxial growth of MoS<sub>2</sub>, while rougher *p*-GaN (roughness of 16.56 nm) cannot result in aligned MoS<sub>2</sub> growth (see Figure S2 in the Supporting Information). By increasing the growth temperature, the MoS<sub>2</sub> forms larger triangular flakes. Statistical calculations of the domain size distribution and the nucleation density are subsequently determined (Figure 2b). All the three histograms exhibit a Gaussian-distribution shape, showing the average domain sizes of  $0.37 \pm 0.22$ ,  $1.11 \pm 0.60$ , and  $1.46 \pm 0.66$  μm at the growth temperatures of 650, 700, and 725 °C, respectively (see the SEM images in Figure S3 in the Supporting Information). As the domain size increases, the surface nucleation density decreases correspondingly. This implies that the growth temperature plays a significant role in facilitating the synthesis of large-scale high-quality MoS<sub>2</sub> single-layers with less grain boundaries. Moreover, by varying the precursor vapor pressure through adjusting the substrate distance from the MoO<sub>3</sub> precursor, the MoS<sub>2</sub> coverage can be elegantly controlled from 10 to near 90% (see Figure S4 in the Supporting Information). The atomic force microscope (AFM) height image of the MoS<sub>2</sub> triangular domains exhibits a nearly homogeneous

color contrast, indicating the uniformity of sample thickness. The line profile of a typical MoS<sub>2</sub> domain (Figure 2c) shows a thickness of about 0.712 nm, confirming the single-layer nature of the samples. Additionally, neither SEM nor AFM images show any stitches or flake overlaps at places where expanding triangles merge to form large-area single-layers. The merging of neighboring MoS<sub>2</sub> triangles without grain boundaries is a prerequisite for the large-area epitaxial 2D material growth. Atomical resolution characterization to resolve the grain boundaries, if there are any, is worthy of further study.

For the ultrathin 2D materials, Raman spectroscopy is a powerful tool that is typically used to determine the number of layers and provide insight into the electron–phonon interaction, doping level, strain, crystal phases, etc. In the as-grown MoS<sub>2</sub>/GaN heterostructure, two distinctive Raman peaks of MoS<sub>2</sub>, the in-plane vibration mode E<sub>2g</sub><sup>1</sup> ( $\approx 385.2$  cm<sup>-1</sup>), and the out-of-plane vibration mode A<sub>1g</sub> ( $\approx 405.7$  cm<sup>-1</sup>) are clearly observed (Figure 2d). The difference between the two peaks is 20.5 cm<sup>-1</sup>, which corresponds to single-layer MoS<sub>2</sub>.<sup>[22,23]</sup> Surprisingly, we observe an additional strong peak centered at 414.8 cm<sup>-1</sup> labeled by an orange arrow that does not exist in the Raman spectra of either single-layer MoS<sub>2</sub> grown on SiO<sub>2</sub> substrate or pristine GaN. The emerging Raman peak is in accord with the high-order harmonic frequency of an acoustic phonon of GaN,<sup>[15,16]</sup> which is not a Raman active mode. To gain better understanding of the emerging Raman mode, we carried out systematic laser excitation energy-dependent Raman spectroscopy measurements (see Figure S5 in the Supporting Information). The emerging Raman mode shows strong enhancement with excitation energies of 1.92 and 2.09 eV, where the scattered

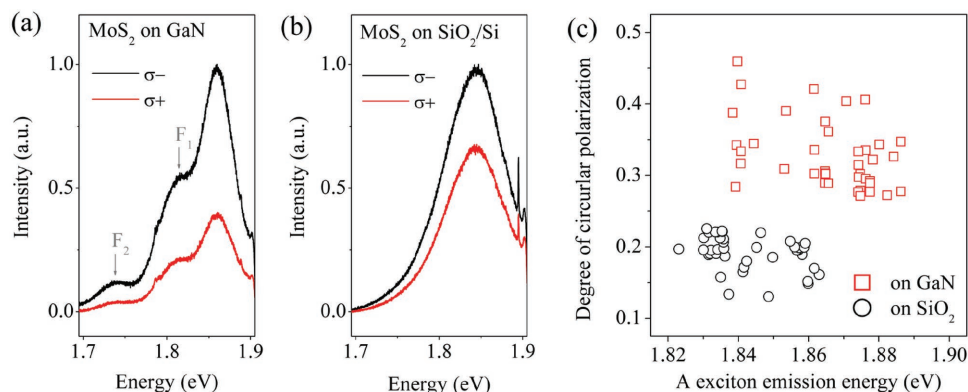


**Figure 3.** a,b) Circularly polarized PL spectra of single-layer MoS<sub>2</sub> on GaN and SiO<sub>2</sub>/Si under 1.96 eV  $\sigma^-$  CW excitation, respectively, at room temperature. The excitation power is 4.8 mW. c) Dependence of degree of circular polarizations on the A exciton emission energies for 40 single-layer MoS<sub>2</sub> samples on GaN and 40 samples on SiO<sub>2</sub>/Si.

photons coincide with the A and B exciton resonances in MoS<sub>2</sub>. In the heterostructure, the vibration modes of the GaN lattice can significantly modulate the carrier behavior of MoS<sub>2</sub>, thus enabling efficient interlayer electron–phonon coupling. As a result, a resonant Raman scattering process emerges that involves both GaN phonon vibrations and MoS<sub>2</sub> electronic resonances, allowing us to observe the new Raman peak.<sup>[24]</sup> The presence of electron–phonon interactions in the MoS<sub>2</sub>/GaN heterostructure can modulate the exciton dynamic relaxation in MoS<sub>2</sub>, and offer a new route to engineer the valley polarization in MoS<sub>2</sub>/substrate heterostructure.

The degree of valley polarization from the single-layer MoS<sub>2</sub>/GaN heterostructure is determined from the polarization-resolved PL spectrum ( $\sigma^-$  and  $\sigma^+$  components), excited by  $\sigma^-$  radiation on resonance with the A exciton at 1.96 eV (633 nm). The excitation power is 4.8 mW (Figure 3a). The fringes at the low energy side result from the GaN thin film interference (see Figure S6 in the Supporting Information). We quantify the degree of PL polarization by the helicity,<sup>[9,12,13]</sup>

$$P = (I_{\sigma^-} - I_{\sigma^+}) / (I_{\sigma^-} + I_{\sigma^+}) \quad (1)$$

where  $I_{\sigma^-}$  and  $I_{\sigma^+}$  are the peak intensities of the left- and right-circularly polarized PL. From statistical analysis of 40 single-layer MoS<sub>2</sub> flakes on GaN,  $P$  is found to be  $0.33 \pm 0.05$  (Figure 3c), indicating the strong valley polarization in the single-layer MoS<sub>2</sub>/GaN heterostructure at room temperature (300 K). In contrast, the PL helicity of the as-grown single-layer MoS<sub>2</sub> on SiO<sub>2</sub> substrate under identical measurement and growth conditions is relatively low ( $0.19 \pm 0.02$ , Figure 3b,c), indicating the 2D material–substrate interaction plays a critical role in the modulation of the valley helicity in single-layer MoS<sub>2</sub>. Statistically, the A exciton emission energy of MoS<sub>2</sub>/GaN is found to be  $1.87 \pm 0.01$  eV, and apparently larger than that of MoS<sub>2</sub>/SiO<sub>2</sub> ( $1.84 \pm 0.01$  eV), due to the well-matched crystal lattice constants and small thermal expansion coefficient discrepancy between MoS<sub>2</sub> and GaN. Plotting the relationship between the A exciton emission energy and the degree of valley polarization (Figure 3c), we find that helicities for MoS<sub>2</sub> on GaN (red squares) and SiO<sub>2</sub> (black circles) collapse into two regions without any noticeable relationship between the A exciton emission energy and the

polarization helicity. Moreover, for two samples with identical A exciton emission energy, the polarization helicity of MoS<sub>2</sub> on GaN is always larger than that on SiO<sub>2</sub>. Generally, resonance pump will result in an increased valley helicity, due to the suppressed phonon-assisted intervalley scattering.<sup>[13,14]</sup> The above results indicate that the phonon-assisted intervalley scattering does not play an important role in the enhancement of the polarization helicity in the MoS<sub>2</sub>/GaN heterostructure.

The polarization helicity,  $P$ , is determined by the ratio between exciton relaxation time ( $\tau$ ) and intervalley scattering time ( $\tau_v$ ), as predicted by a rate equation model:<sup>[9]</sup>  $P = P_0 / (1 + 2\tau/\tau_v)$ , where  $P_0$  is a constant degree of circular polarization depending on optical pumping. Consequently, the enhanced valley helicity observed in single-layer MoS<sub>2</sub> on GaN can be explained by the competition between the intervalley scattering rate and the substrate-induced faster decay rate of the exciton. To accurately extract the  $\tau$  and  $\tau_v$ , we elucidate the valley dynamics by measuring the time-resolved helicity using a synchroscan streak camera. Under a femtosecond pulsed  $\sigma^-$  excitation with the energy of 1.97 eV (630 nm) and excitation power of 80  $\mu$ W, the time-resolved  $\sigma^-$  emission from the K valley shows a higher intensity than that of the  $\sigma^+$  emission from the K' valley for both single-layer MoS<sub>2</sub> on GaN (Figure 4a) and SiO<sub>2</sub> (Figure 4b), confirming the valley-contrasting optical selection rule. Compared with the  $\sigma^-$  polarization emission, the  $\sigma^+$  polarization emission always decays slower until the populations in the two valleys are equal. This difference between the two decay trends results from intervalley scattering, which tends to equalize the exciton populations in the two valleys. Based on the time-integrated intensities,  $I_{\sigma^-}$  and  $I_{\sigma^+}$ ,  $P$  is calculated to be 0.32 and 0.22, respectively, for single-layer MoS<sub>2</sub> on GaN and SiO<sub>2</sub>. These polarization helicities are consistent with those observed values under continuous wave (CW) laser excitation. By deconvolution fitting with the instrument response function (IRF), the differential PL intensity ( $I_{\sigma^-} - I_{\sigma^+}$ ) dynamics spectra (Figure 4c) show the valley lifetime,  $\tau_v$ , to be  $2.1 \pm 0.2$  ps for MoS<sub>2</sub> on GaN and  $1.7 \pm 0.2$  ps for MoS<sub>2</sub> on SiO<sub>2</sub>. There is no great difference in the valley lifetime between these two systems, indicating the 2D material–substrate interaction does not notably modulate the valley scattering process in our system. The total PL intensity ( $I_{\sigma^-} + I_{\sigma^+}$ ) dynamics (Figure 4d) traces

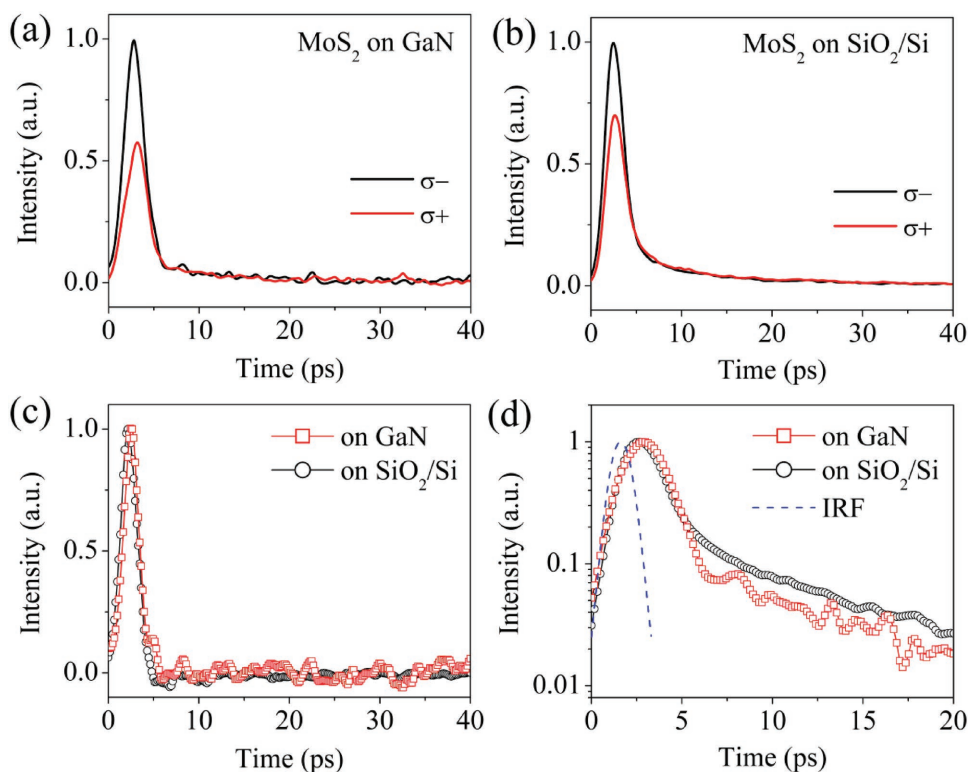


**Figure 4.** a,b) Room-temperature time-resolved circularly polarized PL spectra from single-layer MoS<sub>2</sub> on GaN and SiO<sub>2</sub>/Si, respectively. The excitation is 1.97 eV  $\sigma^-$  polarization femtosecond laser with a power of 80  $\mu$ W. c) Time-resolved differential PL intensities ( $I_{\sigma^-} - I_{\sigma^+}$ ) measured from single-layer MoS<sub>2</sub> on GaN and SiO<sub>2</sub>/Si. Deconvolution fitting with the IRF for the time-resolved valley exciton population can yield the intervalley scattering times. d) Time-resolved total PL intensities ( $I_{\sigma^-} + I_{\sigma^+}$ ) measured from single-layer MoS<sub>2</sub> on GaN and SiO<sub>2</sub>/Si. Deconvolution fitting can yield the exciton lifetimes.

the exciton relaxation and recombination processes. Based on a single exponential decay equation, we can obtain an effective exciton lifetime of  $1.4 \pm 0.2$  ps for single-layer MoS<sub>2</sub> on GaN. However, the normalized time-resolved PL intensity obtained from MoS<sub>2</sub>/SiO<sub>2</sub> can only be fitted based on a double exponential decay equation as:  $I(t) = I_1 \exp(-t/\tau_1) + I_2 \exp(-t/\tau_2)$ , where  $\tau_1$  and  $\tau_2$  are two time constants for decay paths,  $I_1$  and  $I_2$  are the corresponding amplitude of the PL intensity. With the fitted values of  $\tau_1$ ,  $\tau_2$ ,  $I_1$ , and  $I_2$  of  $1.0 \pm 0.2$  ps,  $12.6 \pm 0.4$  ps, 0.56, and 0.44, respectively, we can obtain an effective exciton lifetime of 3.2 ps for single-layer MoS<sub>2</sub> on SiO<sub>2</sub>. With a similar intervalley

scattering rate, the faster exciton decay rate will lead to a higher polarization helicity. The difference in exciton lifetime between single-layer MoS<sub>2</sub> on GaN and SiO<sub>2</sub> is overwhelming enough to cause the enhanced valley helicity observed in the MoS<sub>2</sub>/GaN heterostructure. The ability to manipulate the single-layer TMDCs valley dynamics with an underlying substrate opens new opportunities for valley-sensitive 2D materials photonics and optoelectronics.

In order to interpret the faster exciton decay rate, we performed SKPM and UPS measurements to gain insight into the band alignment of the MoS<sub>2</sub>/GaN heterojunction. The SKPM

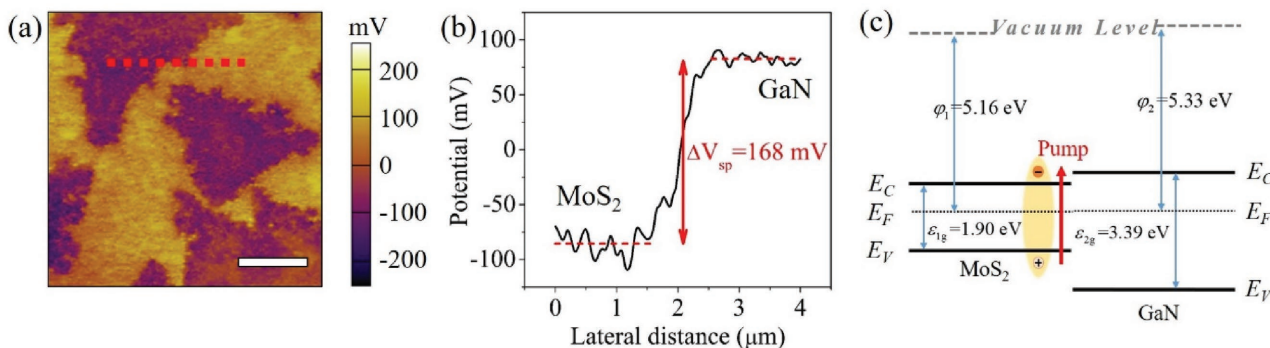


**Figure 5.** a) SKPM image of single-layer MoS<sub>2</sub> on GaN. Scale bar: 2  $\mu$ m. b) Surface potential profile across the MoS<sub>2</sub>/GaN interface. A surface potential difference of  $\approx 168$  mV between the GaN and single-layer MoS<sub>2</sub> is obtained. c) The energy band alignment of MoS<sub>2</sub>/GaN interface.

image displays a clear surface potential contrast between single-layer MoS<sub>2</sub> and GaN substrate (Figure 5a). From the potential profile across the MoS<sub>2</sub> edge (Figure 5b), we obtain a surface potential difference of ≈168 mV between the GaN and single-layer MoS<sub>2</sub>. The sample surface potential can be obtained by  $\phi_{\text{sample}} - \phi_{\text{tip}} = eV_{\text{sp}}$ , where  $\phi_{\text{tip}}$  and  $\phi_{\text{sample}}$  are the work functions of the conductive tip and sample, respectively, and  $V_{\text{sp}}$  is the measured surface potential. After calibrating the tip work function using a gold thin film with a well-known work function of 5.10 eV, we are able to determine the work functions of single-layer MoS<sub>2</sub> and GaN to be 5.16 and 5.33 eV, respectively, which agree well with the results obtained from the UPS measurements (see UPS spectra in Figure S10 in the Supporting Information). Based on the reported bandgaps,<sup>[25,26]</sup> affinities,<sup>[27,28]</sup> and measured work functions of single-layer MoS<sub>2</sub> and GaN, the single-layer MoS<sub>2</sub> and GaN forms a type-I heterojunction (Figure 5c). The band offsets of conduction and valence bands are 0.27 and 1.22 eV, respectively. In this heterojunction, both the conduction band minimum and valence band maximum reside in the single-layer MoS<sub>2</sub>. Therefore, the MoS<sub>2</sub> exciton decay from the charge transfer will not be efficient. Echoing the Raman spectroscopy results, the vibration modes of the GaN lattice can significantly modulate the behavior of electrons and holes in MoS<sub>2</sub> through efficient electron–phonon coupling. The photoexcited carriers generated in MoS<sub>2</sub> are strongly coupled to GaN phonons via the 2D material–substrate interaction, and lose their energy to the crystal lattice by emitting phonons in GaN, which can lead to a much faster exciton decay rate. Consequently, an enhanced valley helicity occurs.

In summary, we have successfully synthesized epitaxial single-layer MoS<sub>2</sub> on lattice-matched GaN substrates via the CVD method. The electron–phonon interaction between single-layer MoS<sub>2</sub> and GaN substrate dynamically modulates the valley polarization, resulting in an enhanced valley helicity of  $0.33 \pm 0.05$  at room temperature. Understanding and further controlling such interlayer 2D material–substrate interaction will not only advance our fundamental knowledge of 2D material–substrate systems, but also help us to manipulate single-layer TMDCs valley dynamics. Our work opens new opportunities for valley-sensitive 2D materials based photonics and optoelectronics.

## Experimental Section

**Sample Preparation:** Single-layer MoS<sub>2</sub> was grown by the CVD method in a dual-temperature-zone system, using S (99.999%, Ourchem) and MoO<sub>3</sub> (99.99%, Ourchem) as sources, pieces of 2 μm GaN/sapphire and 300 nm SiO<sub>2</sub>/Si chips as substrates, and high-purity inert argon as carrier gas. Epitaxial growth of GaN on sapphire was realized by metal-organic chemical vapor deposition.

**Morphology Characterization:** The detailed morphologies of MoS<sub>2</sub> were examined by AFM (Cypher, Asylum Research) and SEM (NanoSEM 430, FEI). The surface potential of the investigated samples were characterized using AFM with the SKPM module.

**Optical Measurement:** The Raman spectra were measured by a confocal Raman microscopicsystem (Labram HR800, Horiba) using a 2.62 eV (473 nm) CW laser as excitation. The laser beam was focused onto the sample by a 100× objective lens. The scattered light was collected and collimated by the same lens. The scattered signals were dispersed by a spectrometer with an 1800 grooves/mm grating and captured by a thermoelectrically cooled charge-coupled device detector at –67 °C. The circular polarized PL spectra were measured by a home-built PL system equipped with a

spectrometer (SR500, Andor), under a resonant excitation energy of 1.96 eV (633 nm), using a HeNe laser. The valley dynamics measurement was done by a synchroscan streak camera. The femtosecond pulsed laser (190 fs, 80 MHz) with an energy of 1.97 eV (630 nm) was used as excitation.

## Supporting Information

Supporting Information is available from the Wiley Online Library or from the author.

## Acknowledgements

This work was supported by the National Key R&D Program of China (Grant No. 2017YFA0206301), the National Basic Research Program of China (Grant No. 2013CB921901), the National Natural Science Foundation of China (Grant Nos. 61521004, 11474007, and 11674005), the King Abdulah University of Science and Technology (KAUST) Office of Sponsored Research (OSR) under Award No. OSR-2016-CRG5-2996, the National Science Foundation (NSF) under grant 1753380, and the “Youth 1000 Talent Plan” Fund. Y.Y. thanks Ting Cao from University of California, Berkeley, for help discussions.

## Conflict of Interest

The authors declare no conflict of interest.

## Keywords

electron–phonon coupling, gallium nitride, single-layer molybdenum disulfide, substrate engineering, valley helicity

Received: July 12, 2017

Revised: September 17, 2017

Published online: December 19, 2017

- [1] D. Jariwala, T. J. Marks, M. C. Hersam, *Nat. Mater.* **2017**, *16*, 170.
- [2] C. Zhao, T. Norden, P. Zhang, P. Zhao, Y. Cheng, F. Sun, J. P. Parry, P. Taheri, J. Wang, Y. Yang, *Nat. Nanotechnol.* **2017**, *12*, 757.
- [3] D. Sarkar, X. Xie, W. Liu, W. Cao, J. Kang, Y. Gong, S. Kraemer, P. M. Ajayan, K. Banerjee, *Nature* **2015**, *526*, 91.
- [4] J. Dai, D. Wang, M. Zhang, T. Niu, A. Li, M. Ye, S. Qiao, G. Ding, X. Xie, Y. Wang, *Nano Lett.* **2016**, *16*, 3160.
- [5] J. Lee, F. Schmitt, R. Moore, S. Johnston, Y. T. Cui, W. Li, M. Yi, Z. Liu, M. Hashimoto, Y. Zhang, *Nature* **2014**, *515*, 245.
- [6] F. Katmis, V. Lauter, F. S. Nogueira, B. A. Assaf, M. E. Jamer, P. Wei, B. Satpati, J. W. Freeland, I. Eremin, D. Heiman, *Nature* **2016**, *533*, 513.
- [7] K. F. Mak, K. L. McGill, J. Park, P. L. McEuen, *Science* **2014**, *344*, 1489.
- [8] J. Lee, K. F. Mak, J. Shan, *Nat. Nanotechnol.* **2016**, *11*, 421.
- [9] T. Cao, G. Wang, W. Han, H. Ye, C. Zhu, J. Shi, Q. Niu, P. Tan, E. Wang, B. Liu, J. Feng, *Nat. Commun.* **2012**, *3*, 887.
- [10] Q. Ji, Y. Zhang, T. Gao, Y. Zhang, D. Ma, M. Liu, Y. Chen, X. Qiao, P. H. Tan, M. Kan, *Nano Lett.* **2013**, *13*, 3870.
- [11] Z. Song, Z. Li, H. Wang, X. Bai, W. Wang, H. Du, S. Liu, C. Wang, J. Han, Y. Yang, *Nano Lett.* **2017**, *17*, 2079.
- [12] H. Zeng, J. Dai, W. Yao, D. Xiao, X. Cui, *Nat. Nanotechnol.* **2012**, *7*, 490.

- [13] K. F. Mak, K. He, J. Shan, T. F. Heinz, *Nat. Nanotechnol.* **2012**, *7*, 494.
- [14] G. Kioseoglou, A. T. Hanbicki, M. Currie, A. L. Friedman, D. Gunlycke, B. T. Jonker, *Appl. Phys. Lett.* **2012**, *101*, 221907.
- [15] H. Siegle, G. Kaczmarczyk, L. Filippidis, A. P. Litvinchuk, A. Hoffmann, C. Thomsen, *Phys. Rev. B* **1997**, *55*, 7000.
- [16] V. Y. Davydov, Y. E. Kitaev, I. N. Goncharuk, A. N. Smirnov, J. Graul, O. Semchinova, D. Uffmann, M. B. Smirnov, A. P. Mirgorodsky, R. A. Evarestov, *Phys. Rev. B* **1998**, *58*, 12899.
- [17] H. L. Liu, C. C. Chen, C. T. Chia, C. C. Yeh, C. H. Chen, M. Y. Yu, S. Keller, S. P. Denbaars, *Chem. Phys. Lett.* **2001**, *345*, 245.
- [18] R. Murray, B. Evans, *J. Appl. Crystallogr.* **1979**, *12*, 312.
- [19] R. R. Reeber, K. Wang, *J. Mater. Res.* **2011**, *15*, 40.
- [20] D. Ruzmetov, K. Zhang, G. Stan, B. Kalanyan, G. R. Bhimanapati, S. M. Eichfeld, R. A. Burke, P. B. Shah, T. P. O'Regan, F. J. Crowne, A. G. Birdwell, J. A. Robinson, A. V. Davydov, T. G. Ivanov, *ACS Nano* **2016**, *10*, 3580.
- [21] J. Liao, B. Sa, J. Zhou, R. Ahuja, Z. Sun, *J. Phys. Chem.* **2014**, *118*, 17594.
- [22] S. L. Li, H. Miyazaki, H. Song, H. Kuramochi, S. Nakaharai, K. Tsukagoshi, *ACS Nano* **2012**, *6*, 7381.
- [23] G. Plechinger, J. Mann, E. Preciado, D. Barroso, A. Nguyen, J. Eroms, C. Schüller, L. Bartels, T. Korn, *Semicond. Sci. Technol.* **2014**, *29*, 064008.
- [24] C. Jin, J. Kim, J. Suh, Z. Shi, B. Chen, X. Fan, M. Kam, K. Watanabe, T. Taniguchi, S. Tongay, *Nat. Phys.* **2016**, *13*, 127.
- [25] K. F. Mak, C. Lee, J. Hone, J. Shan, T. F. Heinz, *Phys. Rev. Lett.* **2010**, *105*, 136805.
- [26] M. Suzuki, T. Uenoyama, A. Yanase, *Phys. Rev. B* **1995**, *52*, 8132.
- [27] M. H. Chiu, W. H. Tseng, H. L. Tang, Y. H. Chang, C. H. Chen, W. T. Hsu, W. H. Chang, C. I. Wu, L. J. Li, *Adv. Funct. Mater.* **2017**, *27*, 1603756.
- [28] M. E. Levinshtein, S. L. Rumyantsev, M. S. Shur, *Properties of Advanced Semiconductor Materials: GaN, AlN, InN, BN, SiC, SiGe*, John Wiley & Sons, New York **2001**.